THEORY AND SIMULATION OF REAL AND IDEAL MAGNETOHYDRODYNAMIC TURBULENCE

John V. Shebalin

Advanced Space Propulsion Laboratory
NASA Johnson Space Center
Houston, Texas 77058, USA

1991 *Mathematics Subject Classification.* 76F05, 76F20, 76W05

Keywords and phrases. Homogeneous turbulence, magnetohydrodynamics, broken symmetry, coherent structure.

Running head. MAGNETOHYDRODYNAMIC TURBULENCE

Author contact information. Dr. John V. Shebalin
NASA Johnson Space Center
Mail Code ASPL
Houston, TX 77058

Tel: (281) 792-5390

Fax: (281) 702-5661

Email: j.shebalin@jsc.nasa.gov

ABSTRACT. Incompressible, homogeneous magnetohydrodynamic (MHD) turbulence consists of fluctuating vorticity and magnetic fields, which are represented in terms of their Fourier coefficients. Here, a set of five Fourier spectral transform method numerical simulations of two-dimensional (2-D) MHD turbulence on a 512^2 grid is described. Each simulation is a numerically realized dynamical system consisting of Fourier modes associated with wave vectors $\mathbf{k}$, with integer components, such that $k = |\mathbf{k}| \leq k_{\max}$. The simulation set consists of one ideal (non-dissipative) case and four real (dissipative) cases. All five runs had equivalent initial conditions. The dimensions of the dynamical systems associated with these cases are the numbers of independent real and imaginary parts of the Fourier modes. The ideal simulation has a dimension of 366104, while each real simulation has a dimension of 411712. The real runs vary in magnetic Prandtl number P_M, with $P_M \in \{0.1, 0.25, 1, 4\}$. In the results presented here, all runs have been taken to a simulation time of $t = 25$. Although ideal and real Fourier spectra are quite different at high k, they are similar at low values of k. Their low k behavior indicates the existence of broken symmetry and coherent structure in real MHD turbulence, similar to what exists in ideal MHD turbulence. The value of P_M strongly affects the ratio of kinetic to magnetic energy and energy dissipation (which is mostly ohmic). The relevance of these results to 3-D Navier-Stokes and MHD turbulence is discussed.

1. **Introduction.** Sufficiently energetic continuum flow, whether it consists of liquid, gas, or plasma, tends to develop instabilities that lead to the large-scale chaotic motion called turbulence. Although fluid compression may be present initially, density fluctuations can radiate away as sound waves or damp out due to bulk viscosity, leaving a large-scale flow that is essentially incompressible. This incompressible limit is characterized by its fluid vorticity, and additionally, in the case of plasma, by its magnetic field. Understanding magnetohydrodynamic (MHD) turbulence requires solving the equations describing the evolution of the vorticity and magnetic induction. However, due to the inherent non-linearity of these equations, there are no general analytical solutions (as linear equations have) and they must be solved numerically.

A fundamental focus for research is in an area termed *homogeneous turbulence* [1], where the region of fluid under consideration is assumed to be remote from any physical boundaries. In this case, the appropriate numerical boundaries are periodic and Fourier series are used as the basis for analytical approaches and computational techniques. Fourier transformation turns the few basic partial differential equations describing the flow in physical space (x-space) into many ordinary differential equations (ODEs) in the Fourier transform space (k-space). To enable numerical solution, these ODEs must be finite in number, requiring that finite Fourier series be used. Typically, the truncation is done by retaining only those Fourier modes whose wave vectors $\mathbf{k}$ (with integer components) have magnitudes less than or equal to some maximum value, $k = |\mathbf{k}| \leq k_{\max}$ (for dissipative turbulence $k_{\max} \approx k_D$, the dissipation wave number). The number of independent real and imaginary parts of the Fourier coefficients within the ball $k \leq k_{\max}$ determines the dimension of the dynamical system embodied by these k-space ODEs.

Since each discrete Fourier mode in k-space represents a continuous function in x-space, we have a discrete dynamical system (the Fourier modes) representing, to a certain level of resolution, a continuous physical system. Although the Fourier modes are themselves continuous analytical functions of time, the actual values they can take are discrete, being drawn from the possible digital states of a computer word (of 64 bits in the numerical simulations to be described herein). Thus we have, in computational physics, the unavoidable result that continuum systems are always represented by discrete dynamical systems, consisting, as they do, of algorithms, their numerical implementation, and the digital hardware on which they are run. The viability of these simulations is ultimately determined through comparison with theoretical prediction and experimental measurement.

Here, we will concentrate our efforts on examining certain aspects of two-dimensional, homogeneous, magnetohydrodynamic turbulence (hereafter simply called 2-D MHD turbulence). In particular, we will consider both ideal (non-dissipative) and real (dissipative) 2-D MHD turbulence. In the ideal case, there is a statistical theory with which to compare numerical results [7, 10, 16, 17, 30–37], and in the real cases we compare the distribution of energy with inertial decay laws [14, 24] and with the distribution found in the ideal case. However, we do not add energy through spectral forcing to the real case, so that the dissipative simulations are autonomous dynamical systems [38] in which energy decays with time.

The one ideal and four real cases presented here all start from equivalent initial conditions, so that a controlled comparison can be made. The real cases differ in their values of kinetic viscosity ν and magnetic diffusivity η (so that the runs are identified by their *magnetic Prandtl number*, $P_M = \nu/\eta$). These five runs took about three months of cpu-time on a DEC Alpha, allowing each simulation (with 64-bit words) to be taken up to a simulation time of $t = 25$. (In the future, we plan to extend these times by an order of magnitude to study long-term states of decaying 2-D MHD turbulence with varying P_M; the runs to be presented contain significant new results that motivate this extension).

The growth and quasi-stationarity of low-k modal values in decaying 2-D MHD turbulence, similar to the behavior seen in the ideal case, is a primary result. In particular, in the real runs those Fourier modes with low values of k exhibited manifestations of the dynamically broken symmetry and associated coherent structure that has been found in ideal turbulence [32, 33, 35]. Thus, although the ideal and real Fourier spectra are quite different at high k, their similarity at low-k, indicates an area of overlap between ideal and real MHD turbulence.

These results are also relevant to 3-D homogeneous Navier-Stokes and MHD turbulence. The reason is that homogeneous 2-D and 3-D MHD turbulence, as well as 3-D Navier-Stokes, each have, in addition to energy, an ideal integral invariant called a *helicity* [2, 6, 23, 39]. It is the presence of helicity that dynamically breaks the symmetry of the basic equations[32, 33, 35]. (The ideal invariants for homogeneous 2-D Navier-Stokes turbulence are energy and enstrophy, neither of which is helical.) In this regard, 2-D MHD turbulence serves as representative of 3-D turbulence, one that allows a substantially greater k_{max} than possible in 3-D simulations.

In outline, the following sections contain a brief, but thorough discussion of the basic MHD equations, their 2-D form, and their 2-D integral invariants. Fourier transforms are then discussed, along with some aspects of 2-D MHD turbulence as a dynamical system. Next, the statistical mechanics of ideal 2-D MHD turbulence, the spectral laws for real turbulence, the numerical method and results, and finally, concluding remarks are presented.

2. **Basic equations.** The first of the basic equations of MHD turbulence is the *Navier-Stokes equation* with the electromagnetic force term $\mathbf{j}\times\mathbf{B}$ [20, 28] (where $\mathbf{j}$ is the electric current and $\mathbf{B}$ is the magnetic induction):

$$\rho\left(\frac{\partial \mathbf{u}}{\partial t} + \mathbf{u}\cdot\nabla\mathbf{u}\right) = -\nabla p + \mu\nabla^2\mathbf{u} + \mathbf{j}\times\mathbf{B} \qquad (1)$$

Here, ρ is the mass density, p is the pressure and μ is the dynamic viscosity. The dynamic viscosity is related to the kinematic viscosity ν through $\mu = \rho\nu$. The assumption of incompressibility means that $\rho = \rho_o$ = constant or equivalently that $\nabla\cdot\mathbf{u} = 0$.

The magnetic evolution equation originates in Maxwell's equations [12], which in SI (Système International) units (*i.e.*, the MKSA system), are

$$\text{a)}\ \frac{\partial \mathbf{B}}{\partial t} = -\nabla \times \mathbf{E} \qquad \text{b)}\ \nabla \cdot \mathbf{B} = 0 \tag{2}$$

$$\text{a)}\ \frac{\partial \mathbf{D}}{\partial t} = \nabla \times \mathbf{H} - \mathbf{j} \qquad \text{b)}\ \nabla \cdot \mathbf{E} = \rho_e \tag{3}$$

Above we have the electric *field* **E**, the electric *displacement* **D**, the magnetic *field* **H** and the magnetic *induction* **B**. We assume that the fluid is neither dielectric nor permeable, so that the electric variables **E** and **D** are related through the free space electric permittivity ε_o, and the magnetic variables **H** and **B** are related through the free space magnetic permeability μ_o (both ε_o and μ_o are constants), while a simple form of Ohm's law connects **j** and **E** (here, the electrical conductivity σ is assumed constant):

$$\text{a)}\ \mathbf{D} = \varepsilon_o \mathbf{E} \qquad \text{b)}\ \mathbf{B} = \mu_o \mathbf{H} \qquad \text{c)}\ \mathbf{j} = \sigma \mathbf{E}\,. \tag{4}$$

In MHD, incompressibility implies that velocities are small with respect to the speed of sound and therefore also to the speed of light. Thus, electromagnetic radiation is ignored, so that on the left side of (3a) the *displacement current* $\partial \mathbf{D}/\partial t$ is set to zero. (Since the addition of the displacement current was Maxwell's unifying, in dropping it, (2) and (3) become the 'no yet Maxwell equations' [12])

Neglecting the displacement current in (3a) and using (4b) gives the relation between electric current and magnetic induction:

$$\mu_o \mathbf{j} = \nabla \times \mathbf{B}. \tag{5}$$

Obviously, $\nabla \cdot \mathbf{j} = 0$, so that both **B** and **j** have zero-divergence.

Now, combining Faraday's law of magnetic induction (2a), Ohm's law (4c), and the current-magnetic induction relation (5), yields the second basic equation of MHD, the *magnetic induction equation*:

$$\frac{\partial \mathbf{B}}{\partial t} = \nabla \times (\mathbf{u} \times \mathbf{B}) + \eta \nabla^2 \mathbf{B}\,. \tag{6}$$

The magnetic diffusivity $\eta = (\mu_o \sigma)^{-1}$ is also a constant (η and ν have the same units: m^2/s in SI units). In MHD, equation (6) determines **B** and '**B** determines **j**' through equation (5), rather than the usual '**j** determines **B**' of Maxwellian electrodynamics.

Equations (1) and (6) are the basic equations of MHD. Since incompressibility is assumed, the system of equations can be non-dimensionalized, so that the constant ρ is

eliminated from (1). The pressure p is removed from consideration by taking the curl of equation (1) (with $\rho = 1$) to yield an equation for the vorticity $\boldsymbol{\omega} = \nabla\times\mathbf{u}$ of the magneto-fluid:

$$\frac{\partial \boldsymbol{\omega}}{\partial t} = \nabla\times\left(\mathbf{u}\times\boldsymbol{\omega} + \mathbf{j}\times\mathbf{B}\right) + \nu\nabla^2\boldsymbol{\omega} \tag{7}$$

The pressure, if required, can be found by taking the divergence of (1).

Equations (6) and (7) are the basic equations of MHD turbulence. In (7), the inverse of ν is the Reynolds number, while in (6) the inverse of η is the *magnetic Reynolds number*. Note that all of the fields **u**, $\boldsymbol{\omega}$, **B** and **j** appearing in (6) and (7) have zero divergence. In the case of **B**, this leads to the well known magnetic vector potential **A**, *i.e.*, $\mathbf{B} = \nabla\times\mathbf{A}$.

3. **2-D MHD.** In the presence of a constant, externally imposed uniform magnetic induction $\mathbf{B}_0$, the total induction **B** can be split into $\mathbf{B}_0$ and a fluctuating part **b**:

$$\text{a)}\ \mathbf{B} = \mathbf{B}_0 + \mathbf{b} \qquad \textbf{b)}\ \nabla\cdot\mathbf{b} = 0. \tag{8}$$

In 3-D cartesian coordinates x, y, z, the corresponding orthonormal basis vectors are $\hat{\mathbf{e}}_x$, $\hat{\mathbf{e}}_y$, $\hat{\mathbf{e}}_z$, respectively. Let us choose $\mathbf{B}_0 = B_0\hat{\mathbf{e}}_z$. In the limit $B_0 \to \infty$, with fixed limits on fluctuating magnetic and kinetic energies, equations (6) and (7) give

$$\text{a)}\ \frac{\partial}{\partial t}\begin{pmatrix}\mathbf{j}\\ \boldsymbol{\omega}\end{pmatrix} = B_0\frac{\partial}{\partial z}\begin{pmatrix}\boldsymbol{\omega}\\ \mathbf{j}\end{pmatrix} \qquad \text{b)}\ \pm\boldsymbol{\omega} = \mathbf{j} = \mathbf{f}(x, y, z \pm V_A t)\,. \tag{9}$$

The *Alfvén velocity* is $V_A = B_0$ in these dimensionless equations. If the solutions (9b) represent initially localized disturbances in an infinite medium, they propagate away, leaving a 2-D flow field. In the case of a bounded flow, such as homogeneous MHD turbulence, there is nowhere to go. However, in physical experiments [40] and in numerical simulations [30, 31, 25], MHD turbulence has been seen to lose its z dependence for increasing B_0. Thus, in the limit of large $\mathbf{B}_0$, 3-D MHD turbulence becomes effectively 2-D, and the use of 2-D simulations to represent physical phenomena becomes viable.

Also, a 2-D approach is advantageous numerically, since a denser grid can be used than is the case in 3-D. For example, if we use a 512×512 grid in 2-D, we have 512 points per dimension, or 2^{18} points overall. In 3-D, the same number of points would be distributed evenly into a 64×64×64 grid, but with only ⅛ as many points along each dimension. Hence, restricting MHD to 2-D, in addition to being appropriate in the presence of a very large mean magnetic field, also allows for a greatly increased spatial resolution. For these reasons, we now develop and then numerically solve the 2-D MHD equations.

Since $\nabla\cdot\mathbf{b} = \nabla\cdot\mathbf{j} = \nabla\cdot\mathbf{u} = \nabla\cdot\boldsymbol{\omega} = 0$, we can define for 2-D MHD the following:

$$\text{a)}\ \boldsymbol{\psi} = \psi(x,y,t)\hat{\mathbf{e}}_z \qquad \text{b)}\ \mathbf{a} = a(x,y,t)\hat{\mathbf{e}}_z \tag{10}$$

$$\text{a)}\ \mathbf{u} = \nabla\times\boldsymbol{\psi} = -\hat{\mathbf{e}}_z\times\nabla\psi \qquad \text{b)}\ \mathbf{b} = \nabla\times\mathbf{a} = -\hat{\mathbf{e}}_z\times\nabla a. \tag{11}$$

The quantity $\psi(x,y,t)$ is the *stream function* and $a(x,y,t)$ is the *magnetic scalar potential.* In terms of these, the vorticity and current are

$$\text{a)}\ \omega = \nabla\times\mathbf{u} = \omega\hat{\mathbf{e}}_z \qquad \text{b)}\ \mathbf{j} = \nabla\times\mathbf{b} = j\hat{\mathbf{e}}_z \tag{12}$$

$$\text{a)}\ \omega = -\nabla^2\psi \qquad \text{b)}\ j = -\nabla^2 a. \tag{13}$$

If we now put the expressions (10) through (13) into (7) and (6), we get

$$\frac{\partial\omega}{\partial t} + \mathbf{u}\cdot\nabla\omega = \mathbf{b}\cdot\nabla j + \nu\nabla^2\omega \tag{14}$$

$$\frac{\partial a}{\partial t} + \mathbf{u}\cdot\nabla a = \eta\nabla^2 a\,. \tag{15}$$

In these equations, the spatial derivatives are only taken with respect to x and y, *e.g.*,

$$\mathbf{u}\cdot\nabla a = \frac{\partial a}{\partial x}\frac{\partial\psi}{\partial y} - \frac{\partial a}{\partial y}\frac{\partial\psi}{\partial x} \equiv J(a,\psi) \tag{16}$$

$$\nabla^2 a = \frac{\partial^2 a}{\partial x^2} + \frac{\partial^2 a}{\partial y^2}\,. \tag{17}$$

The basic equations of 2-D MHD turbulence are (15) and (16). Since we assume homogeneity, the various scalar fields a, ψ, j and ω are expanded in terms of truncated Fourier series, and Fourier transformation takes the two partial differential equations (14) and (15) into a great number of ordinary differential equations. We will move on to this topic in the next section.

First, however, we will demonstrate the existence of *integral invariants* in a periodic domain in x-space. It is straightforward to show, using (11a), that the Navier-Stokes equation (1) (with $\rho = 1$) can be written as

$$\frac{\partial\nabla\psi}{\partial t} = -\omega\hat{\mathbf{e}}_z\times\nabla\psi - \hat{\mathbf{e}}_z\times\nabla\left(p + \tfrac{1}{2}u^2\right) + j\hat{\mathbf{e}}_z\times\nabla a - \nu\nabla\omega\,. \tag{18}$$

Taking the gradient of (16) gives a similar equation for ∇a:

$$\frac{\partial \nabla a}{\partial t} = J(\nabla\psi, a) + J(\psi, \nabla a) - \eta \nabla j \tag{19}$$

At this point, we take the dot product of (18) with $\nabla\psi$, and of (19) with ∇a, and adding the results, to get the energy flux equation:

$$\text{a)}\quad \frac{\partial \varepsilon}{\partial t} = -\nabla \cdot \left[p_u \mathbf{u} + (\mathbf{u}\cdot\nabla a)\nabla a\right] - \nu \nabla\psi \cdot \nabla\omega - \eta \nabla a \cdot \nabla j \tag{20}$$

$$\text{a)}\quad \varepsilon = \tfrac{1}{2}(|\mathbf{u}|^2 + |\mathbf{b}|^2) \qquad \text{b)}\quad p_u = p + \tfrac{1}{2}u^2 \tag{21}$$

Next, a times (15) plus ω times (16) gives

$$\frac{\partial a\omega}{\partial t} + \nabla \cdot (a\omega\mathbf{u} - aj\mathbf{b}) = \nu a \nabla^2 \omega - \eta \omega j\,. \tag{22}$$

Lastly, a times (16) yields

$$\frac{\partial a^2}{\partial t} + \nabla \cdot (a^2 \mathbf{u}) = -2\eta a j\,. \tag{23}$$

Now, we integrate (20), (22) and (23) over a periodic square of side length 2π, to find the volume averages of the quantities ε, $a\omega$ and a^2, respectively. The volume average of any quantity q will be defined as

$$[q] \equiv (2\pi)^{-2} \int_0^{2\pi} dy \int_0^{2\pi} dx\; q(x,y)\,. \tag{24}$$

All of the divergence terms will vanish because of the periodic boundary condition and the terms containing ν and η can be integrated by parts. The results are

$$\frac{dE}{dt} = -2(\nu\Omega + \eta J) \tag{25}$$

$$\text{a)}\quad E = [\varepsilon] \qquad \text{b)}\quad \Omega = \tfrac{1}{2}[\omega^2] \qquad \text{c)}\quad J = \tfrac{1}{2}[j^2]\,. \tag{26}$$

$$\frac{dH_C}{dt} = -(\nu + \eta) H_J \tag{27}$$

$$\text{a)}\quad H_C = \tfrac{1}{2}[a\omega] \qquad \text{b)}\quad H_J = \tfrac{1}{2}[j\omega] \tag{28}$$

$$\frac{dA}{dt} = -2\eta E_m \tag{29}$$

$$\text{a) } A = \tfrac{1}{2}[a^2] \qquad \text{b) } E_M = \tfrac{1}{2}[|\mathbf{b}|^2]. \tag{30}$$

For completeness, we also define

$$\text{a) } E_K = \tfrac{1}{2}[|\mathbf{u}|^2] \qquad \text{b) } E = E_K + E_M. \tag{31}$$

In the above equations, E is the total mean energy, while E_K and E_M are the mean kinetic and magnetic energies, respectively. The mean squared vorticity is Ω (called the *enstrophy*), while J and A are the *mean squared current* and *mean squared magnetic potential*, respectively. The integral H_C is called the *cross helicity*, while H_J is also a helicity (*i.e.*, a pseudoscalar integral), though it is not an ideal invariant.

If we set the viscosity and diffusivity equal to zero, $\nu = \eta = 0$, we have *ideal* MHD. In this case, equations (25), (27) and (29) tell us that E, H_C and A are integral invariants. In fact, these are the only ideal invariants in 2-D MHD (and they remain so when the fields a and ω are represented by truncated Fourier series, as will be demonstrated presently). If $\nu \neq 0$ and $\eta \neq 0$, we have *real* MHD, wherein E and A decay monotonically, while H_C may increase or decrease. In what follows, we present results from numerical simulations of both ideal and real MHD turbulence. First, however, we discuss the transformation to k-space and the explicit dynamical systems that ensue.

4. **Fourier transform methods.** In x-space, 2-D MHD turbulence is represented by the value of its fields $a(\mathbf{x})$ and $\omega(\mathbf{x})$ (and the fields analytically related to these) within an area of side length 2π, where the position vector is $\mathbf{x} = x\hat{\mathbf{e}}_x + y\hat{\mathbf{e}}_y$, with $0 \leq x,y \leq 2\pi$. Since $a(\mathbf{x})$ and $\omega(\mathbf{x})$ are assumed to be periodic in this area they will be represented by discrete Fourier series, *e.g.*:

$$\text{a) } \omega(\mathbf{x}) = \tfrac{1}{N}\sum_{\mathbf{k}} \tilde{\omega}(\mathbf{k}) e^{i\mathbf{k}\cdot\mathbf{x}} \qquad \text{b) } \omega(\mathbf{k}) = \tfrac{1}{N}\sum_{\mathbf{x}} \tilde{\omega}(\mathbf{x}) e^{-i\mathbf{k}\cdot\mathbf{x}}. \tag{32}$$

Note that time t is implicit in the arguments of all variables such as $a(\mathbf{x})$ and $\tilde{a}(\mathbf{k})$, being omitted only for brevity. Also, $N = 2^M$ for use in fast-Fourier transforms (FFTs) [4]. Here, we use 2-D wave vectors $\mathbf{k}$, with integer components k_x and k_y:

$$\text{a) } \mathbf{k} = k_x\hat{\mathbf{e}}_x + k_y\hat{\mathbf{e}}_y \qquad \text{b) } -\tfrac{N}{2} < k_x, k_y \leq \tfrac{N}{2}. \tag{33}$$

The x-space position vectors $\mathbf{x}$ is transform (32b) are also discrete:

$$\text{a) } \mathbf{x} = \tfrac{2\pi}{N}(n\hat{\mathbf{e}}_x + m\hat{\mathbf{e}}_y) \qquad \text{b) } 0 \leq n, m < N. \tag{34}$$

The x-space values $\omega(\mathbf{x})$ are real, so the Fourier coefficients satisfy the 'reality condition' $\omega(\mathbf{k}) = \omega^*(-\mathbf{k})$, where * denotes complex conjugation[henceforth we drop the $\tilde{}$ over $a(\mathbf{k})$, $\omega(\mathbf{k})$, etc.]. Thus, (32), (33) and (34) define an invertible transformation between N^2 values $\omega(\mathbf{x})$ and the N^2 values $Re\,\omega(\mathbf{k})$, $Im\,\omega(\mathbf{k})$ [and similarly for $a(\mathbf{k})$].

In a numerical implementation, we wish to maintain isotropy in k-space and to avoid aliasing effects in the evaluation of the non-linear terms in (15) and (16). Thus, we require that $|\mathbf{k}| \le k_{\max} < N/2$, which imposes what is termed *isotropic truncation* in k-space for an N-by-N transformation. For a real (dissipative) non-linear simulations, $k^2_{\max}$ is chosen as $(N/2)^2 - \frac{1}{2}$; in these *pseudospectral* simulations [3, 5, 9], dissipation renders aliasing effects negligible. In the case of an ideal simulation, a de-aliasing procedure is required to evaluate non-linear terms; we use the method due to Patterson and Orszag [27] , in which $k^2_{\max} = 2N^2/9$, to create a *Fourier spectral transform method* [3, 5, 9].

Fourier transformation of the non-linear evolution equations (15) and (16) produces the following two equations in k-space:

$$\frac{d\omega(\mathbf{k})}{dt} = i \sum_{\mathbf{p}+\mathbf{q}=\mathbf{k}} \hat{\mathbf{e}}_z \cdot \mathbf{p}\times\mathbf{q}\left[\psi(\mathbf{p})\omega(\mathbf{q}) + j(\mathbf{p})a(\mathbf{q})\right] - \nu k^2 \omega(\mathbf{k}) \tag{35}$$

$$\frac{da(\mathbf{k})}{dt} = i \sum_{\mathbf{p}+\mathbf{q}=\mathbf{k}} \hat{\mathbf{e}}_z \cdot \mathbf{p}\times\mathbf{q}\, a(\mathbf{p})\psi(\mathbf{q}) - \eta k^2 a(\mathbf{k})\,. \tag{36}$$

If we multiply (35) by $\psi^*(\mathbf{k})$ and (36) by $j^*(\mathbf{k})$, and sum over $\mathbf{k}$ (all sums are such that $|\mathbf{k}|$, $|\mathbf{p}|$, $|\mathbf{q}| \le k_{\max}$) we have

$$\frac{dE}{dt} = \theta(\psi,\psi,\omega) + \theta(\psi, j, a) + \theta(a, j, \psi) - 2(\nu\Omega + \eta J) \tag{37}$$

$$\theta(a, j, \psi) = -i \sum_{\mathbf{p}+\mathbf{q}+\mathbf{k}=0} \hat{\mathbf{e}}_z \cdot \mathbf{p}\times\mathbf{q} a(\mathbf{k}) j(\mathbf{p})\psi(\mathbf{q})\ . \tag{38}$$

In the triple summation in (38), $\mathbf{k}$, $\mathbf{p}$ and $\mathbf{q}$ are dummy summation variables and can be interchanged to yield

$$\theta(a, j, \psi) = -\theta(j, a, \psi) = -\theta(a, \psi, j)\,. \tag{39}$$

Thus the three θ terms in (37) add to zero and we find that equation (25) also holds for a truncated Fourier representation. We can similarly multiply (35) by $a^*(\mathbf{k})$ and (36) by $\omega^*(\mathbf{k})$ and add the results, and separately multiply (36) by $a^*(\mathbf{k})$, and sum these over $\mathbf{k}$ to show that (27) and (29) are also valid in for truncated Fourier representations. Therefore, in the ideal case ($\nu = \eta = 0$), E, H_C and A are also invariants in k-space,

$$E = \frac{1}{2N^2}\sum_{\mathbf{k}} k^2[|\psi(\mathbf{k})|^2 + |a(\mathbf{k})|^2] \tag{40}$$

$$\text{a) } H_C = \frac{1}{2N^2}\sum_{\mathbf{k}} a(-\mathbf{k})\omega(\mathbf{k}) \qquad \text{b) } A = \frac{1}{2N^2}\sum_{\mathbf{k}} |a(\mathbf{k})|^2 . \tag{41}$$

(Note that each $\Sigma_{\mathbf{k}}$ sums independent coefficients twice.) The properties of the θ summations, as given by (38) and (39), ensure that E, H_C and A are the only quadratic invariants present in the truncated Fourier representation of 2-D homogeneous MHD turbulence. (If an *ad hoc* constant magnetic field were put into the 2-D problem, then A would no longer be conserved. We will not consider this situation further here.)

5. **MHD Turbulence as a dynamical system.** In 2-D k-space, where $\mathbf{k}$ has integer components, there are a finite number of $\mathbf{k}$ such that $|\mathbf{k}| \le k_{\max}$, and so there are a finite number of independent real and imaginary parts of the coefficients $a(\mathbf{k})$ and $\omega(\mathbf{k})$. This number (call it N_Γ) is the dimension of the phase space Γ of the dynamical system associated with the truncated Fourier model of 2-D MHD turbulence. Since the equations of motion of the phase flow are (35) and (36), the divergence of the phase flow is

$$\text{a) } \frac{\partial\dot{\omega}(\mathbf{k})}{\partial\omega(\mathbf{k})} = -\nu k^2 \qquad \text{b) } \frac{\partial\dot{a}(\mathbf{k})}{\partial a(\mathbf{k})} = -\eta k^2 . \tag{42}$$

Clearly, for ideal MHD where $\nu = \eta = 0$, the phase flow is divergenceless and the quantities E, H_C and A are conserved. The *canonical distribution function* D [19] for phase points satisfies a continuity equation

$$\frac{\partial D}{\partial t} + \sum_{\mathbf{k}}\left[\frac{\partial D\dot{\omega}(\mathbf{k})}{\partial\omega(\mathbf{k})} + \frac{\partial D\dot{a}(\mathbf{k})}{\partial a(\mathbf{k})}\right] = 0 . \tag{43}$$

Using equations (42) allows (43) to be written as

$$\frac{dD}{dt} = \frac{\partial D}{\partial t} + \sum_{\mathbf{k}}\left[\dot{\omega}(\mathbf{k})\frac{\partial D}{\partial\omega(\mathbf{k})} + \dot{a}(\mathbf{k})\frac{\partial D}{\partial a(\mathbf{k})}\right] = (\nu+\eta)\left(\sum_{\mathbf{k}} k^2\right)D . \tag{44}$$

This tells us that if phase space is filled with points representing the initial states of systems [with values of E, H_C and A given by (40) and (41) depending on initial location], then the density of points in any volume moving with the phase flow increases exponentially with time, *i.e.*, the gas of phase points collapses towards the origin, and the associated phase volume shrinks, when ν and η are positive definite constants.

6. Ideal MHD turbulence

6.1. **Absolute equilibrium ensemble theory.** When $\nu = \eta = 0$, however, $dD/dt = 0$ and a *Liouville theorem* exists [21] Thus, since D is a constant function of the phase coordinates $a(\mathbf{k})$ and $\omega(\mathbf{k})$, it can only be a function of other phase functions which are themselves constant: $D = D(E, H_C, A)$. Since E, H_C and A are additive, and since D must be multiplicative when the phase system Γ is split into parts Γ_1 and Γ_2 (*i.e.*, $D = D_1 D_2$) the form of D must be [19]

$$\text{a) } D = Z^{-1}\exp(-\alpha E - \beta H_C - \gamma A) \qquad \text{b) } Z = \int \exp(-\alpha E - \beta H_C - \gamma A)\, d\Gamma. \tag{45}$$

Here α, β and γ are called inverse temperatures and the normalizing factor Z^{-1} is given in terms of the *partition function* Z. Equations (45) describe the statistical mechanics of a *canonical ensemble* [13, 19]. The partition function is a product of modal partition functions $z_R(\mathbf{k})$ and $z_I(\mathbf{k})$ and the volume is a product of modal volumes:

$$\text{a) } Z = \prod_{\mathbf{k}} z_R(\mathbf{k})\, z_I(\mathbf{k}) \qquad \text{b) } d\Gamma = \prod_{\mathbf{k}} d\Gamma_R(\mathbf{k}) d\Gamma_I(\mathbf{k}) \tag{46}$$

$$d\Gamma_S(\mathbf{k}) = da_S(\mathbf{k}) d\omega_S(\mathbf{k}), \quad S = R, I \tag{47}$$

$$z_R(\mathbf{k}) = z_I(\mathbf{k}) = \int \exp[-\alpha(k^{-2}\omega^2 + k^2 a^2) - \beta a\omega - \gamma a^2]\, d\omega da. \tag{48}$$

The subscripts R, I in (48) denote real and imaginary parts, respectively. Expressions (40) and (41) for E, H_C and A are inserted in (45b) to produce (48), where the dummy variables of integration have been simplified. The integrations in (48) are performed between the limits $-\infty$ and $+\infty$ for each a and ω. The partition function thus depends on α, β, γ, and k^2. Carrying out the integrations, we find

$$z_S(\mathbf{k}) = \frac{\pi}{\sqrt{\alpha^2 - \beta^2/4 + \alpha\gamma/k^2}}, \quad S = R, I. \tag{49}$$

Let us define the expectation value of a phase quantity ϕ as follows:

$$\langle\phi\rangle = Z^{-1} \int \phi \exp(-\alpha E - \beta H_C - \gamma A)\, d\Gamma. \tag{50}$$

Using the relations developed above, for $\phi = \omega$ or a, it can be shown that

$$\text{a) } \langle\omega(\mathbf{k})\rangle = 0 \qquad \text{b) } \langle a(\mathbf{k})\rangle = 0. \tag{51}$$

Canonical ensemble theory thus predicts that the mean values of the Fourier coefficients are zero. Second-order moments are also easily found to be

$$\langle [\omega_S(\mathbf{k})]^2 \rangle = \frac{\alpha k^2 + \gamma}{2(\alpha^2 - \beta^2/4 + \alpha\gamma/k^2)}, \quad S = R, I \tag{52}$$

$$\langle [a_S(\mathbf{k})]^2 \rangle = \frac{\alpha/k^2}{2(\alpha^2 - \beta^2/4 + \alpha\gamma/k^2)}, \quad S = R, I \tag{53}$$

$$\langle \omega_S(\mathbf{k}) a_S(\mathbf{k}) \rangle = \frac{-\beta/4}{\alpha^2 - \beta^2/4 + \alpha\gamma/k^2}, \quad S = R, I. \tag{54}$$

The values α, β and γ are found by placing the expressions (52), (53) and (54) into (40) and (41), assuming E, H_C and A are constant and solving the resulting nonlinear equations.

The ideal results presented above form what is called *absolute equilibrium ensemble theory* for 2-D MHD turbulence [10, 18]. (If an *ad hoc* uniform mean field $\mathbf{B}_0$ is introduced into the 2-D case, A is no longer an invariant, although E and H_C remain so [30, 31].) In addition to these ideal 2-D MHD results, there are corresponding formulas for 3-D MHD turbulence [7, 32, 33, 37], as well as 2-D [17, 32, 33] and 3-D [16, 32, 33] Euler (*i.e.*, 'ideal Navier-Stokes') turbulence. In 3-D MHD, the ideal invariants are E, H_C and the *magnetic helicity* [6, 23] $H_M = \frac{1}{2}[\mathbf{a}\cdot\mathbf{b}]$ (if $\mathbf{B}_0 \neq 0$, H_M is no longer invariant [33]). In 2-D homogeneous Euler turbulence, the integral invariants are E and Ω [17], while in 3-D homogeneous Euler turbulence, E and the *kinetic helicity* [2, 23] $H_K = \frac{1}{2}[\mathbf{u}\cdot\boldsymbol{\omega}]$ are invariant. The presence of at least one ideal invariant helicity in each case unites 2-D MHD with 3-D turbulence.

Absolute equilibrium ensemble theory is a straightforward and useful application of Gibbsian statistical mechanics. The initial formulation of the absolute equilibrium theory, developed in the 1970s [7, 10, 16, 17] has been extended in several ways [30–35. These extensions and their uses are described in the following sections.

6.2. **Entropy.** In the ideal case, if the expectation values of (40) and (41) are taken, and (52), (53) and (54) are used, three algebraic equations result:

$$\alpha\langle E\rangle + \beta\langle H_C\rangle + \gamma\langle A\rangle = \frac{N_\Gamma}{2N^2} \equiv n_\Gamma \tag{55}$$

$$2\alpha\langle H_C\rangle + \beta\langle E_M\rangle = 0 \tag{56}$$

$$\alpha(\langle E\rangle - 2\langle E_M\rangle) - \gamma\langle A\rangle = 0. \tag{57}$$

In the above, the expectation values $\langle E\rangle$, $\langle H_C\rangle$ and $\langle A\rangle$ have essentially their initial values E, H_C and A because these have only minor canonical fluctuations. The value $\langle E_M\rangle$ will, however fluctuate significantly since it is not an ideal invariant. Rename this

as $\varphi = \langle E_M \rangle$, for brevity. Then, solving the exactly determined equations (55), (56) and (57) for the unknown φ gives [30, 32, 33]

$$\text{a)}\ \alpha = \frac{n_\Gamma \varphi}{\varphi(E-\varphi) - H_C^2} \qquad \text{b)}\ \beta = -2\frac{H_C \alpha}{\varphi} \qquad \text{c)}\ \gamma = \frac{E-2\varphi}{A}\alpha . \tag{58}$$

Now, instead of having three variables to solve for, there is just one: φ. If the inverse temperatures in (58) are put into the distribution function D in (45), the result is $D(\varphi)$, which is equal to the true distribution function when the equilibrium value of φ is found.

The method for determining φ is to minimize the *entropy functional* $\sigma(\varphi) = -\langle \ln D(\varphi) \rangle$, with respect to φ. Note that although entropy increases as previously isolated systems come together and interact, the entropy of an isolated system takes a minimum value with respect to temperature [13] (or temperatures, as in this case [34]). Equations (58) show that the inverse temperatures are really functions of only one variable, so that minimizing with respect to α, β and γ is equivalent to minimizing with respect to φ. Using (50) and (58), along with (40) and (41) gives

$$\sigma(\varphi) = -\langle \ln D(\varphi) \rangle = n_\Gamma (1 + N^2 \ln \pi) - \tfrac{1}{2}\sum_{\mathbf{k}} \ln(\alpha^2 - \tfrac{1}{4}\beta^2 + \alpha\gamma\, k^{-2}) \tag{59}$$

Again, α, β and γ are functions of φ as given in (58). Finding the value of φ for which minimizes $\sigma(\varphi)$ (there is only one minimum [36]) allows the equilibrium values of α, β and γ to be found, and hence the expectation values (52), (53), and (54). This value is $\varphi = \langle E_M \rangle$, and the entropy of the dynamical system is $S = \sigma(\langle E_M \rangle)$.

6.3. **Broken ergodicity.** The helicities H_C, H_M and H_K, mentioned above have one critical characteristic: they are *pseudoscalars* (*i.e.*, they change sign) under either one or both of the symmetry transformations P (*parity*: $\mathbf{x} \rightarrow -\mathbf{x}$, so that $\mathbf{u}, \mathbf{a}, \mathbf{j} \rightarrow -\mathbf{u}, -\mathbf{a}, -\mathbf{j}$, but $\psi, \mathbf{b}, \omega \rightarrow \psi, \mathbf{b}, \omega$) and C (*charge reversal*: $\mathbf{a}, \mathbf{b}, \mathbf{j} \rightarrow -\mathbf{a}, -\mathbf{b}, -\mathbf{j}$). However, the equations of motion, such as (14) and (15) [or (35) and (36)], are unaffected by P or C. Also, although the distribution function D as given by (45) appears to be affected by P or C, it is not, for the inverse temperature β associated with H_C is clearly a pseudoscalar under P or C, as is seen in (58b), where $\beta = -2H_C\alpha/\varphi$ (α and $\varphi = E_M$ are scalars, while H_C is a pseudoscalar). Similar relations can also be shown to exist for the invariant helicities in 3-D ideal MHD and Euler turbulence [32, 33].

Thus, both the equations of motion and the statistical theory are invariant under P and C. However, in any solution of the ideal equations of motion the various invariant helicities always start with a definite sign (+ or –) and, because they *are* invariant, maintain that sign. In regard to ideal homogeneous turbulence as a dynamical system, each invariant helicity induces a disjoint structure on the available regions of phase space [35]. In ideal 2-D MHD and 3-D MHD with $\mathbf{B}_0 \neq 0$, as well as in 3-D Euler turbulence, there is one invariant helicity so that the available phase space is split into two effectively disjoint

parts. In 3-D MHD turbulence with $\mathbf{B}_0 = 0$, there are two invariant helicities and the available phase space is effectively split into four disjoint parts. Only in the case of 2-D Euler turbulence, where there are no invariant helicities, is there a single, connected part in phase space for the system point to move on [32].

The phrase *effectively disjoint* is used above because in a canonical ensemble, as we have here, invariant surfaces in phase space are actually 'fuzzy,' *i.e.*, the phase point is not precisely confined the to invariant hypersurface Γ_I of dimension $N_I = N_\Gamma - 3$ defined by the intersection of the $N_\Gamma - 1$ dimensional hypersurfaces of precisely constant E, H_C and A. (If phase motion were confined to Γ_I we would have a *microcanonical* ensemble [13, 19].) Instead, E, H_C and A are *canonically invariant*, as they have very small fluctuations about a mean value, similar to the energy of a small physical system embedded in a large thermal heat bath (the 'heat bath' here is the digital computer). The invariant hypersurface Γ_I is thus slightly spread out into an N_Γ dimensional subspace $\Delta\Gamma$ in which the phase point resides with a probability given by the integral $\int_{\Delta\Gamma} D d\Gamma \cong 1$, where D is the canonical distribution function given in (45). Since D is so highly peaked on Γ_I, the probability that the phase point can actually be found between the effectively disjoint subspaces $\Delta\Gamma_\pm$ ($\Delta\Gamma = \Delta\Gamma_+ \cup \Delta\Gamma_-$) associated with $\pm H_C$ is essentially zero.

Numerical simulation has demonstrated the disjoint nature of phase space for ideal turbulence when invariant helicities are present [32, 33, 35]. Although (51) predicts that the mean values of $\omega(\mathbf{k})$ and $a(\mathbf{k})$ zero for 2-D MHD turbulence, in any dynamical simulation time averages of these modal values are no longer zero. The phase point begins and remains within one disjoint part of phase space, while ensemble averages are taken over all of phase space consistent with the canonically invariant values of E, $|H_C|$ and A. Thus, the symmetry of the governing equations and statistical theory under P and C is *dynamically broken* and the dynamical system is *non-ergodic* (as time averages do not match ensemble averages). This situation is often referred to as *broken ergodicity* [26]. Since the time-averaged values of $\omega(\mathbf{k})$ and $a(\mathbf{k})$ are no longer zero, these time averages define the existence of a *coherent structure*.

The essential result is that direct numerical simulation of ideal, homogeneous turbulence is described by a dynamical system with a canonical distribution function. Furthermore, the presence of helical invariants induces broken ergodicity and coherent structure. Does this ideal turbulent phase space structre manifest itself in real turbulence when ν and η are non-zero? This is an important question that we will address presently. First, a brief discussion of real turbulence is given.

7. **Real MHD turbulence.** In real 2-D MHD turbulence, when $\nu \neq 0$, $\eta \neq 0$, the spectrum is expected to be quite different from (52), (53) and (54). For forced, dissipative turbulence, a stationary state can be attained by injecting energy at some small value of k, after which it cascades through intermediate values of k with negligible dissipation (the *inertial range*), and is lost to heat at large k in the dissipation range, where $k > k_D$, the dissipation wave number. (There can also be 'inverse cascades' to the smallest values of k.) The kinetic energy spectrum $E_K(k)$ and magnetic energy spectrum $E_M(k)$ are defined as integrals over azimuthal angle ϕ in k-space:

$$E_K(k) = \tfrac{1}{2}\int_0^{2\pi} |\,\mathbf{u}(\mathbf{k})\,|^2\; k d\phi = \frac{\pi}{k}\,|\,\omega(\mathbf{k})\,|^2_{ave} \tag{60}$$

$$E_M(k) = \tfrac{1}{2}\int_0^{2\pi} |\,\mathbf{b}(\mathbf{k})\,|^2\; k d\phi = \frac{\pi}{k}\,|\,j(\mathbf{k})\,|^2_{ave} \tag{61}$$

In the case of homogeneous Navier-Stokes turbulence, Kolmogorov [14] and Obukhov [24] used a dimensional arguments to predict that in the inertial range

$$E_K(k) \approx k^{-5/3}. \tag{62}$$

For MHD turbulence with a mean field $\mathbf{B}_0 \neq 0$, Iroshnikov [11] and Kraichnan [15] have predicted that Alfvén wave effects produce inertial range spectra of the form

$$E_K(k) \approx E_M(k) \approx k^{-3/2}. \tag{63}$$

Here, we have no explicit mean field, since a large $\mathbf{B}_0$ was invoked only to turn 3-D into 2-D MHD turbulence, so that (62) should apply here, rather than (63).

In the later stages of decay, theory [1] predicts a specific form for the energy spectrum $E_K(k)$ of homogeneous Navier-Stokes turbulence. Since the equations for velocity and induction are the same when the non-linear terms are neglected, the magnetic energy spectrum $E_M(k)$ of homogeneous MHD turbulence will take a similar form. The spectra for the later stages of decay (*i.e.*, as $t \to 0$) are thus expected to behave as

$$\text{a)}\;\; E_K(k) \approx k^4 \exp(-2\nu k^2 t) \qquad \text{b)}\;\; E_M(k) \approx k^4 \exp(-2\eta k^2 t). \tag{64}$$

Finally, the dissipation wave number k_D for MHD turbulence can be approximated as (through dimensional reasoning similar to the Navier-Stokes case)

$$k_D = 2\pi\left(\frac{\nu^2}{2\Omega} + \frac{\eta^2}{2J}\right)^{-1/4}. \tag{65}$$

The above results pertaining to both ideal and real turbulence can be used to examine some new 'computer experiments.'

8. **Numerical Simulation.** We solve the k-space ordinary differential equations (35) and (36) for $\omega(\mathbf{k})$ and $a(\mathbf{k})$ with $|\mathbf{k}| \leq k_{\max}$ and reset all coefficients with $|\mathbf{k}| > k_{\max}$ to zero after each time step (*isotropic truncation*). Let the number of $\mathbf{k}$ (with integer components not all zero) in the ball $|\mathbf{k}| \leq k_{\max}$ be K. Associated with each of these $\mathbf{k}$ is one $a(\mathbf{k})$ and one $\omega(\mathbf{k})$. Since $a^*(\mathbf{k}) = a(-\mathbf{k})$ and $\omega^*(\mathbf{k}) = \omega(-\mathbf{k})$, the number of wave vectors with independent coefficients is $K/2$. Since each $a(\mathbf{k})$ or $\omega(\mathbf{k})$ has a real and an imaginary part,

the number of dimensions in the phase space is $N_\Gamma = 4K/2 = 2K$. Approximately, we have $K \cong \pi k^2_{\max}$, although the exact number requires summation (this is *Gauss's circle problem*), and numerical counting can arrive at precise values of K.

Here, we present recent numerical simulations performed on an $N \times N$ grid of points with $N = 512$. Time integration is done by a third-order 'partially corrected Adams-Bashforth' scheme [8], and the linear dissipative terms are treated implicitly. Spatial differentiation is performed in k-space, where it is simple multiplication since the x-space $\nabla \rightarrow \mathbf{ik}$ in k-space. Non-linear terms are evaluated by a) finding derivatives within cofactors in k-space, b) transforming these cofactors to x-space by fast Fourier transform (FFT), c) forming products at each point in x-space into Jacobians [such as $J(a,\psi)$ given by (16)] and d) transforming back to k-space by FFT. The *aliasing* that may occur in this transform method is fully eliminated in ideal runs by the Patterson-Orszag technique [27], where each evaluation of a non-linear term requires two sets of FFTs on shifted grids (this is a *spectral method* with $k^2_{\max} = 2N^2/9$). The effects of aliasing are neglected in real runs (with only onset of FFTs per evaluation – this is a *pseudospectral method* with $k^2_{\max} = \frac{1}{4}N^2 - \frac{1}{2}$). Thus, for $N = 512$, ideal runs have $k^2_{\max} = 58254$ and $K = 183052$ ($\pi k^2_{\max} = 183010$ – low by 42), while real runs have $k^2_{\max} = 65535$ and $K = 205856$ ($\pi k^2_{\max} = 205884$ – high by 28).

The simulation set consists of one ideal case and four real cases. All five runs had equivalent initial conditions (*i.e.*, equal for $k^2 \leq 58254$). The dimension of the dynamical system in all cases is again $N_\Gamma = 2K$. Thus, $N_\Gamma = 366104$ in the ideal simulation, and $N_\Gamma = 411712$ in the real simulations. Table I gives the values of ν, η and the magnetic Prandtl number $P_M = \nu/\eta$ for each of these five runs (the ideal case is denoted by $P_M =$ '0/0').

Run	ν	η	P_M
I1	0	0	0/0
R1	0.001	0.010	0.10
R2	0.001	0.004	0.25
R3	0.0025	0.0025	1.00
R4	0.004	0.001	4.00

Table I. Parameters for the numerical simulations

The initial conditions were such that $E_K = E_M = 0.5$, $H_C = 0.024613$, $A = 0.031031$ at $t = 0$. The initial values of the complex coefficients $\omega(\mathbf{k})$ and $j(\mathbf{k})$ had random phase and magnitudes that varied as

$$|\omega(\mathbf{k})| = |j(\mathbf{k})| \sim k^3 \exp(-k^2/16). \tag{66}$$

These initial values gave initial energy spectra $E_K(k) = E_M(k) \sim k^6 \exp(-k^2/8)$, *i.e.*, one that was highly peaked around $k^2 = 5$. The time step for numerical integration was $\Delta t = 10^{-4}$, and each run in Table I was taken to $t = 25$. Each time step for the ideal run took about 9 cpu-seconds, while the time steps for the real runs took about 5 seconds each.

Thus, the total cpu-time invested (on a DEC Alpha running a 64-bit Fortran code named *mhd2.f*) was approximately 2000 cpu-hours and the run-time memory required was 66.4 Mbytes.

9. **Numerical Results.** First, the initial and time-averaged values, as well as standard deviations (as percentages of the time averages) of E, H_C, A and E_M for the ideal run are given in Table 2.

Integral	Initial	Time average	Std. Dev.
E	1.0000	1.0004	0.02 %
H_C	0.024613	0.024603	0.03 %
A	0.031031	0.031031	2×10^{-5} %
E_M	0.50000	0.56045	6.35 %

Table 2. Integral invariants for the ideal run ($P_M = 0/0$); averages from $t = 0$ to 25.

Upon using the average values in Table 2 for E, H_C and A, a minimum for the entropy defined in equation (59) is found to occur at $\varphi = \langle E_M \rangle = 0.515678$. Using (58) then gives values to the inverse temperatures of $\alpha = 1.4371$, $\beta = -0.13713$, and $\gamma = -1.4334$. Putting these values into (52) and (53) allows us to predict the ideal spectra. In Figure 1, we compare these predicted spectra with spectra found in the ideal simulation, at times $t = 1$ and $t = 25$. Simulation spectra were found by using (60) and (61), with discrete averaging done in bands around integer values of k_n: $n - \frac{1}{2} \le k_n < n + \frac{1}{2}$, where $k_n = 1, 2, \ldots, [k_{max}]$ (here, $[z]$ is the integer part of the real number z).

It is evident in Figure 1 that the spectra in the ideal run have evolved by $t = 25$ so as to be essentially the same as the predicted spectra at high k. However, they differ at low k, and the question is if and how quickly the low k spectra will collapse to the prediction. Let us look at Figure 2, where the ratio $E_K/E_M = E/E_M - 1$ versus time t is given for the five runs. For the ideal run ($P_M = 0/0$), this ratio does not appear to be approaching $E_M = 0.515678$, *i.e.*, $\log_{10}(E_K/E_M) = -0.0272444$, but rather is approaching $\log_{10}(E_K/E_M) \cong -0.0492$.

The results shown in Figure 2 for $P_M = 0/0$ indicate that the low k coefficients may not evolve into their absolute equilibrium predictions. The value of E_M appears to have become stationary at $t = 20$, and if we average from $t = 20$ to 25, we get the results in Table 3. As before, upon using the average values in Table 3 for E, H_C and A, a minimum for the entropy defined in equation (59) is found to occur at $\varphi = \langle E_M \rangle = 0.515834$. Using (58) then gives values to the inverse temperatures of $\alpha = 1.4366$, $\beta = -0.13699$, and $\gamma = -1.4329$. Putting these values into (52) and (53) allows us again to predict the ideal spectra, which does not perceptively differ from that shown in Figure 1. The predicted value $\langle E_M \rangle = 0.515834$ differs from the time average in Table 3 by more than 10 standard deviations. Thus, there a small but significant departure in the simulation results from the predictions of the absolute equilibrium ensemble theory [7, 10, 16, 17].

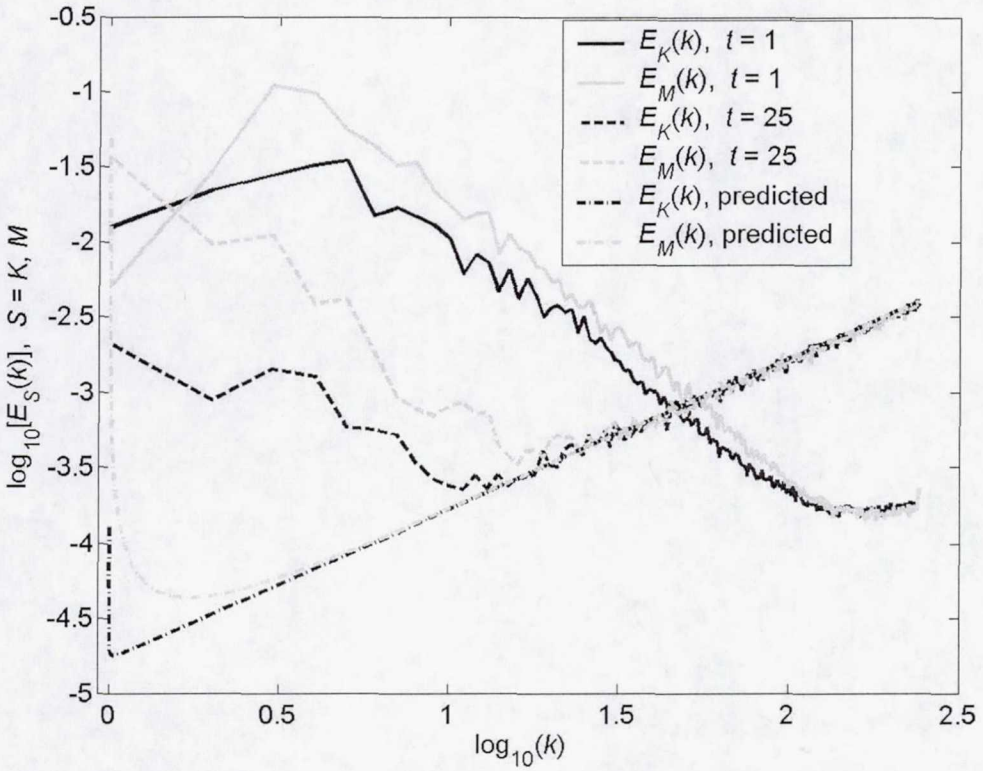

Figure 1. Predicted and simulated ideal spectra.

Figure 2 indicates that E_K/E_M increase with decreasing P_M, *i.e.*, with increasing η. Now, consider the total energy (26a) with respect to time, as shown in Figure 3. The ideal run ($P_M = 0/0$) has constant energy, as it should, while the real runs decay more quickly the lower their value of P_M. Thus decay is directly correlated with magnetic diffusivity η, rather than with kinematic viscosity ν, so that energy loss is primarily ohmic. (In the real runs, the dissipation wave number (59) was $k_D \approx k_{\max}$ at $t \approx 0.5$ and $k_D < k_{\max}$ otherwise.)

The mismatch between absolute equilibrium ensemble theory and numerical simulation in ideal MHD turbulence is, again, caused by the broken ergodicity discussed in Section 6.3. Broken ergodicity is clearly manifested in the time behavior of the coefficients $a(\mathbf{k})$ and $\omega(\mathbf{k})$ for ideal MHD turbulence. In order to see whether a similar effect appears in real MHD turbulence, we plot the evolution of $a(\mathbf{k})$ and $\omega(\mathbf{k})$ for several values of $\mathbf{k}$.

In Figure 4, the time evolution of $a(\mathbf{k})$ for $\mathbf{k} = (0,1)$ is presented for all five runs. In Figure 5, the time evolution of $\omega(\mathbf{k})$, also for $\mathbf{k} = (0,1)$ is shown for all runs. These are the projections of the phase trajectory onto two-dimensional planes. It is clear that the phase trajectory is not even approximately symmetric about the origin. The effect is quite evident for $k = 1$, though it diminishes for higher k. In Figure 6, the time evolution of $a(\mathbf{k})$ (multiplied by k) for $\mathbf{k} = (1,2)$ is presented for all five runs, where the projected phase trajectory does not seem as non-ergodic as for the $k = 1$ cases. In Figure 7, the time

evolution of $\omega(\mathbf{k})$, also for $\mathbf{k} = (-2,2)$ is shown for all runs. In this last figure, the trajectory appears to flow into a more ergodic-looking shape around the origin. It must be remembered that these figures show different two-dimensional projections of a phase trajectory that evolves in a phase space of dimension of 366104 in the ideal run, and a dimension of 411712 in the real runs. The essential result is that the broken ergodicity that exists in ideal MHD turbulence also seems to appear in the real case.

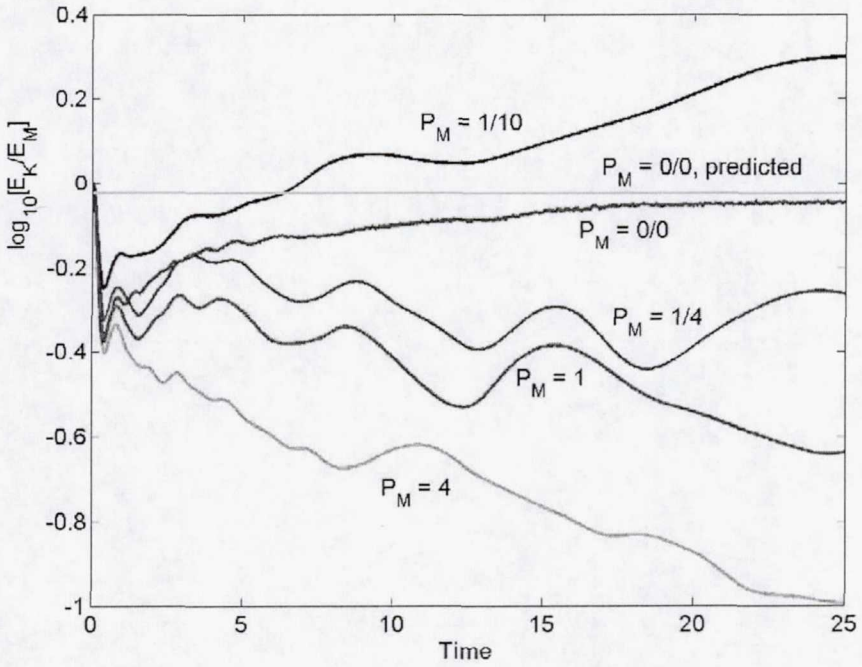

Figure 2. Ratio of E_K to E_M with respect to simulation time.

Integral	Initial	Time average	Std. Dev.
E	1.0000	1.0007	0.004 %
H_C	0.024613	0.024593	0.005 %
A	0.031031	0.031031	0.000 %
E_M	0.50000	0.53037	0.252 %

Table 3. Integral invariants for the ideal run ($P_M = 0/0$); averages from $t = 20$ to 25.

Another result that appears in Figures 4 – 7 is that the low k modes grow in amplitude, while Figure 3 shows that total energy is dissipated in the real runs. Thus, we have an *inverse cascade* [10], in which energy flows to low k modes at the same time it is flowing to high k modes where it is lost. This can be quantified by plotting modal energy $E(k)$ versus time, as is done in Figures 8 for $E(k)$, $k = 1$; in Figure 9 for $E_M(k)$, $k = 1$; and in

Figure 10, for $E(k)$, $k = 5$. Figure 8 shows that the energy for $k = 1$ reaches a stationary state, while Figure 9 shows that the magnitude at $k = 1$ is mostly due to magnetic energy. Figure 10 illustrates the behavior of $E(k)$ for $k = 5$ (and generally for $E(k)$ with $k > 1$), which is to enter a stage of decay by $t = 25$.

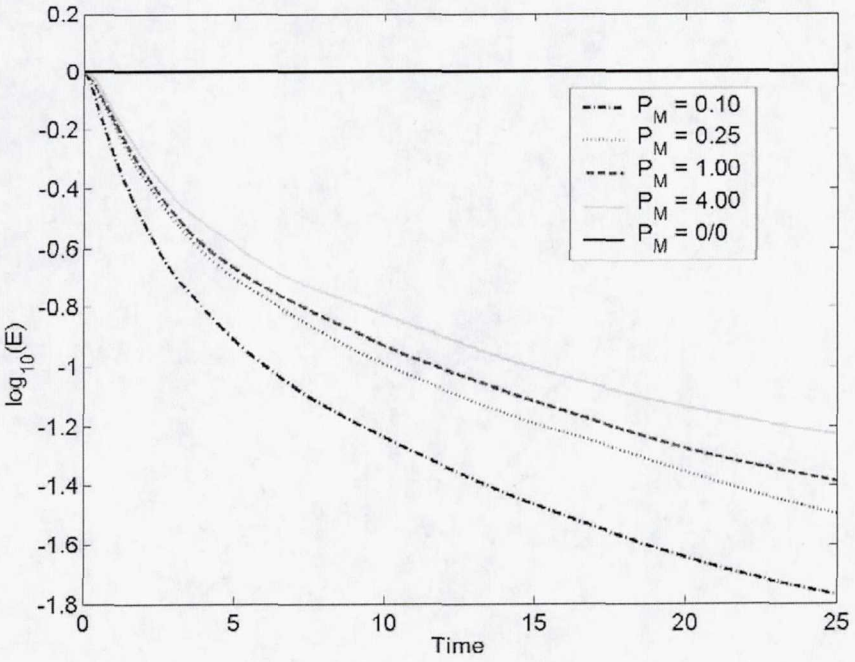

Figure 3. Total energy E with respect to simulation time.

Figures 4 – 10 suggest that the coefficients $a(\mathbf{k})$ and $\omega(\mathbf{k})$ are random variables with non-zero mean values. To examine this further, rolling time-averages and variances of the real and imaginary parts of both $a(\mathbf{k})$ and $\omega(\mathbf{k})$ were kept. Thus, for all coefficients, means and standard deviations were determined from $t = 0$ to $t = 25$. Non-zero mean values give rise to coherent structure, while variances quantify the random fluctuations within MHD turbulence. In the same way that complete coefficients determine kinetic and magnetic energy and spectra, the mean coefficients can be used to find *coherent* energy and spectra, and the variances can be used to find *random* energy and spectra. In Figure 11, coherent and random energy are plotted for the ideal case $P_M = 0/0$, and compared with absolute ensemble predictions. There is clear evidence that a significant amount of coherent energy exists across the whole spectral range, and particularly at low k. Although a more definitive result for this ideal case requires a considerable extension of the run with time, definitive results have been found previously in long runs on 32^2 grids, where significant amounts of coherent energy and structure were first discovered [32].

The more interesting question at this point is the relevance of *ideal* results to *real* MHD turbulence. As Figures 4 –10 show, there is a high degree of similarity at low k between the ideal and real runs presented here (where all runs began with essentially the same initial conditions). We now look at the final energy spectra of these five runs for further evidence of similar behavior. In Figure 12, we see the real and ideal total energy spectra

at $t = 25$, where it is clear that there is great similarity at low k and none at high k. Also, the Kolmogorov-Obukhov law [14,24] $E(k) \sim k^{-5/3}$ has been inserted for comparison.

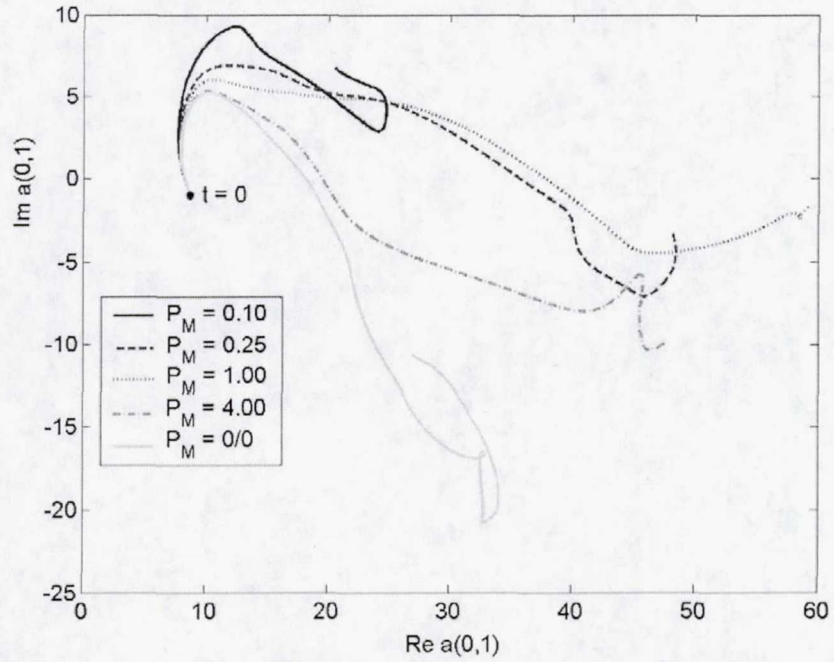

Figure 4. Evolution of $a(\mathbf{k})$, $\mathbf{k} = (0,1)$, for all runs.

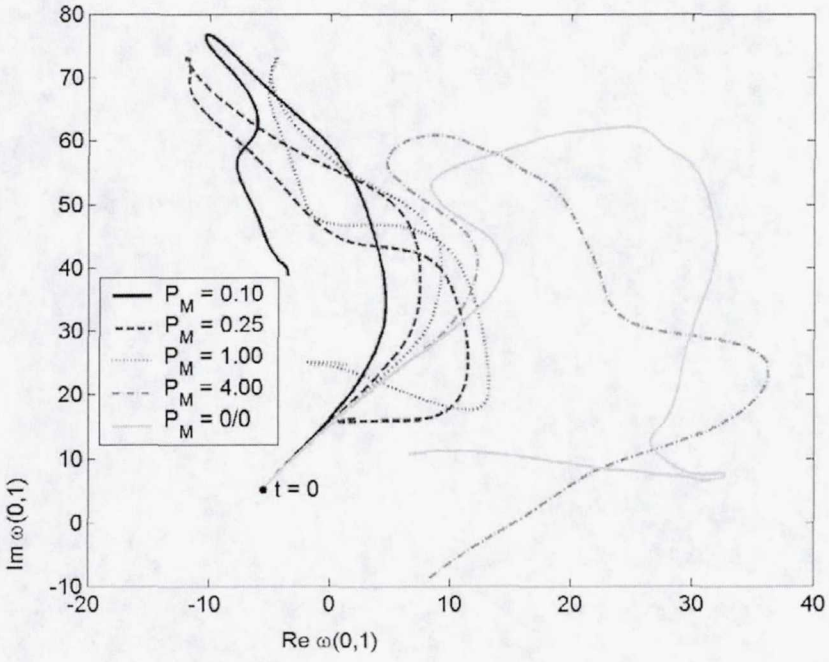

Figure 5. Evolution of $\omega(\mathbf{k})$, $\mathbf{k} = (0,1)$, for all runs.

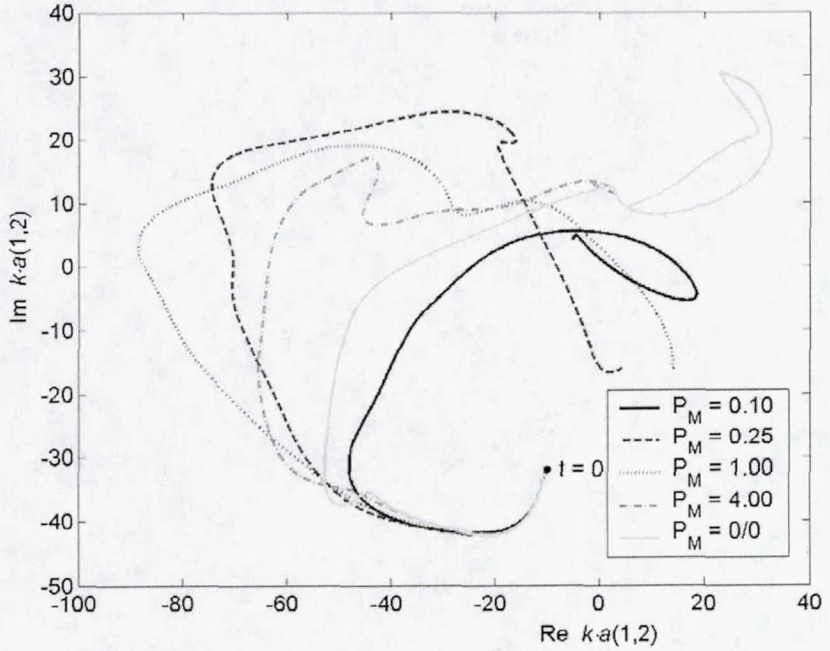

Figure 6. Evolution of $a(\mathbf{k})$, $\mathbf{k} = (1,2)$, for all runs.

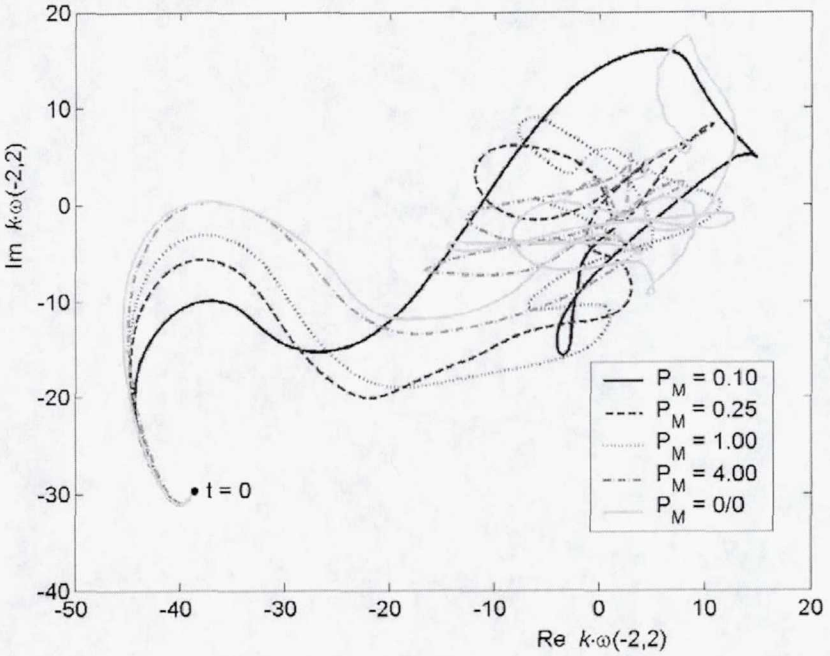

Figure 7. Evolution of $\omega(\mathbf{k})$, $\mathbf{k} = (-2,2)$, for all runs.

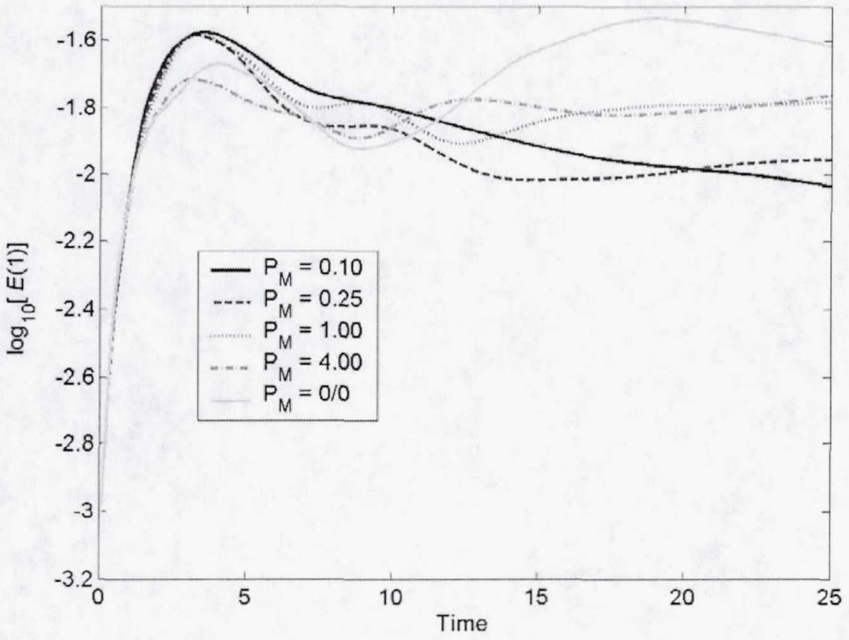

Figure 8. Evolution of $E(k)$, $k = 1$, for all runs.

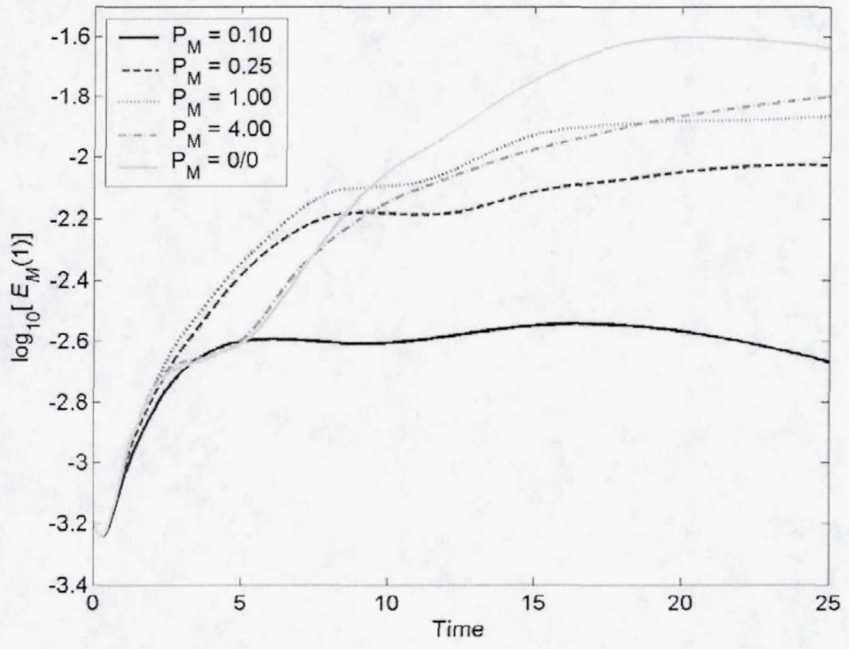

Figure 9. Evolution of $E_M(k)$, $k = 1$, for all runs.

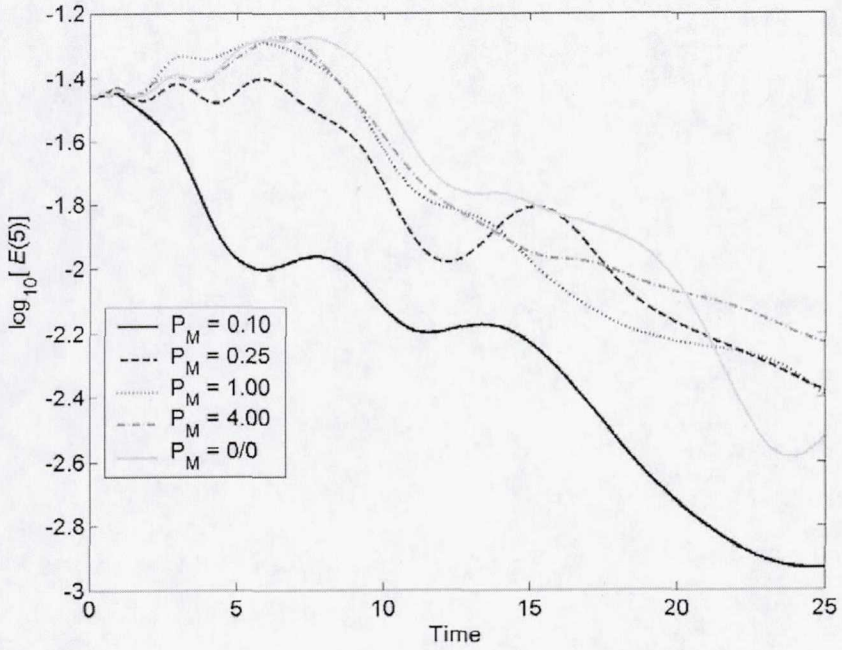

Figure 10. Evolution of $E(k)$, $k = 5$, for all runs.

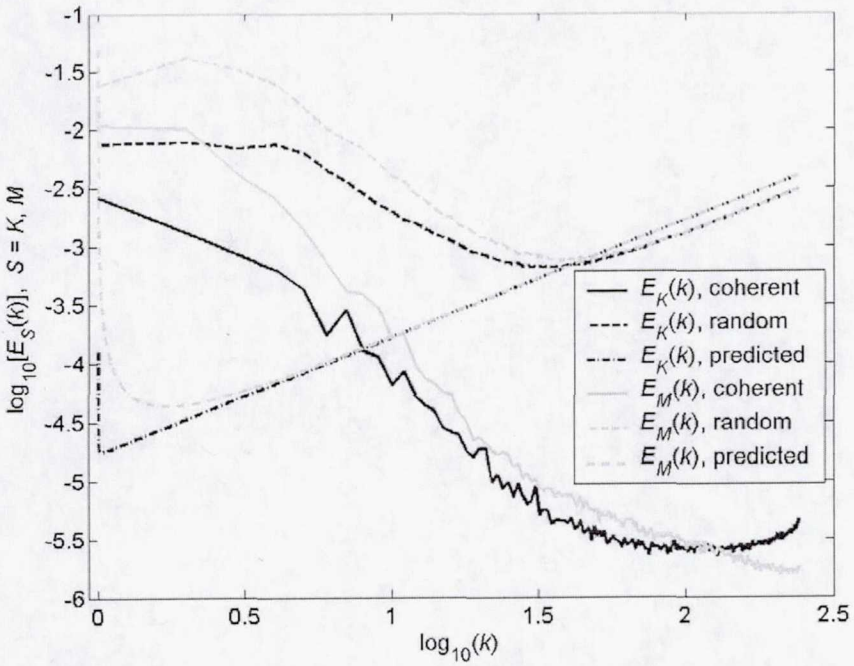

Figure 11. Coherent and random ideal spectra from time-averaged coefficients.

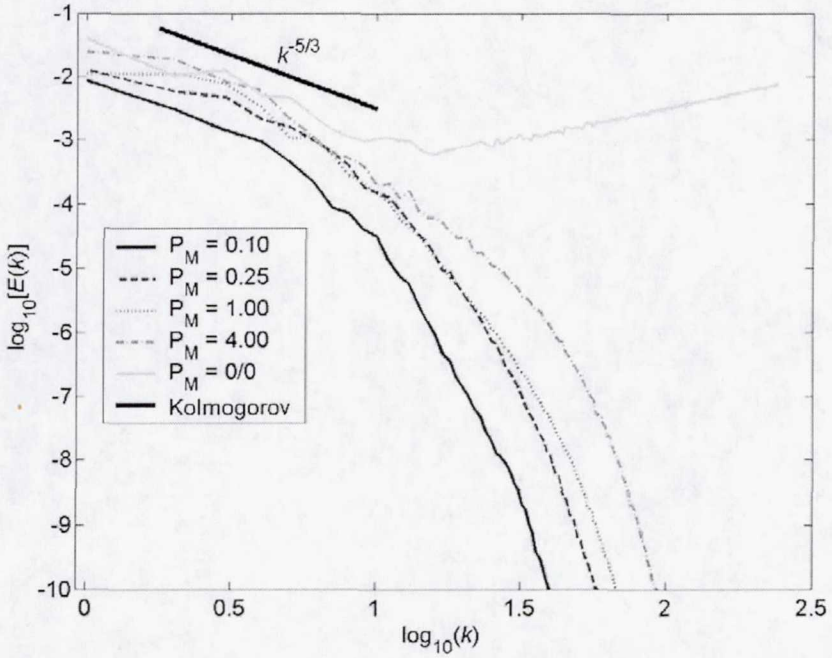

Figure 12. Ideal and real energy spectra at $t = 25$.

10. **Conclusion.** The representation of MHD turbulence by numerically realized finite dynamical systems produces intriguing results. The 'broken ergodicity' that exists in ideal MHD turbulence, and is strongest at low k, appears to have a counterpart in numerical simulations of real MHD turbulence. In fact, the low k behavior of the ideal and real runs presented here show a striking level of similarity. At high k, however, the energy spectra of ideal and real MHD turbulence differ radically. Thus, there is an apparent dichotomy in the in the transition from zero to non-zero values of ν and η. First, ideal and real simulations agree well at low k (where ideal simulations do not agree with absolute ensemble theory due to broken ergodicity). Second, ideal and real simulations disagree at high k (where the ideal simulation agrees well with absolute ensemble theory). It seems as if the coefficients $\omega(\mathbf{k})$ and $a(\mathbf{k})$ at low k are only weakly coupled to the high k part of the spectrum, in both the ideal and real cases. This, in turn, provides a justification for the study of so-called 'large eddy simulations' [29], in which the effects of high k coefficients are replaced by analytical sub-grid scale models.

The result of varying the magnetic Prandtl number also leads to important insights. First, energy dissipation in MHD turbulence is primarily ohmic. Second, equipartion of energy between kinetic and magnetic modes in the real runs occurs at a value of P_M such that $0.10 < P_M < 0.25$, the precise value of which requires extended run times. Lastly, growth and saturation of the $k = 1$ modes appears to depend only weakly on P_M.

Although it is natural to extend simulations such as those presented here to significantly longer run times, the results found in the appear to be robust in light of the evident stationarity achieved during the latter part of these runs. There is much to be done and

there are also aspects of MHD turbulence other than those discussed here that can be profitably studied through numerical simulation. An additional benefit of 2-D MHD turbulence simulations is that these serve as representatives of 3-D MHD and Navier-Stokes turbulence, since these (but not 2-D Navier-Stokes turbulence) all possess at least one ideal invariant helicity, and that these numerical studies allow for higher $k_{\max}$ than possible in 3-D simulations.

While homogeneity is useful theoretical and computational assumptions, physical systems never truly support homogeneous flows. Nevertheless, The numerically observed growth and maintenance of coherent structures at the largest wavelengths is a qualitative feature which may represent a fundamental cause of the tendency of geophysical and astrophysical systems to spontaneously form large scale vortices or magnetic fields. Thus, broken ergodicity in MHD turbulence may well hold the key to understanding, for example, the ubiquitous presence of large scale magnetic fields in our earth, in our sun, and in other planets and stars.

REFERENCES

[1] G. K. Batchelor, The Theory of Homogeneous Turbulence, Cambridge U. P., Cambridge, UK, 1953.

[2] R. Betchov, An invariant integral in fluid turbulence, Phys. Fluids, 4 (1961), 925.

[3] J. P. Boyd, Chebyshev and Fourier Spectral Methods, 2nd Ed., Dover, Mineola, NY, 2001.

[4] R. N Bracewell, The Fourier Transform and its Applications, 2nd Ed., McGraw-Hill, New York, 1986.

[5] C. Canuto, M. Y. Hussaini, A. Quateroni, & T. A. Zang, Spectral Methods in Fluid Dynamics, Springer-Verlag, New York, 1988.

[6] W. M. Elsässer, Hydromagnetic Dynamo Theory, Rev. Mod. Phys., 28 (1956), 135–163.

[7] U. Frisch, A. Pouquet, J. Leorat, & A. Mazure, Possibility of an inverse cascade of magnetic helicity in magnetohydrodynamic turbulence, J. Fluid Mech., 68 (1975), 769–778.

[10] D. Fyfe & D. Montgomery, High beta turbulence in two-dimensional magneto-hydrodynamics, J. Plasma Phys., 16 (1976), 181–191.

[8] J. Gadzag, Time-differencing schemes and transform methods, J. Comp. Phys., 20 (1976), 196.

[9] D. Gottlieb & S. A. Orszag, Numerical Analysis of Spectral Methods: Theory and Applications, SIAM, Philadelphia, 1977.

[10] M. Hossain, Inverse energy cascades in three-dimensional turbulence, Phys. Fluids B, 3 (1991), 511–514.

[11] P. S. Iroshnikov, Turbulence of a conducting fluid in a strong magnetic field, Sov. Astron., 7 (1964), 566–571.

[12] J. D. Jackson, Classical Electrodynamics, 3rd Ed., Wiley, New York (1999), 237–239.

[13] A. I. Khinchin, Mathematical Foundations of Statistical Mechanics , Dover, New York, 1949, 137-145.

[14] A. N. Kolmogorov, Local structure of turbulence in an incompressible fluid at very large Reynolds numbers, Dokl. Akad. Nauk SSSR, 30 (1941), 299–303.

[15] R. H. Kraichnan, Inertial range spectrum in hydromagnetic turbulence, Phys. Fluids, 8, 155 (1965), 1385–1387.

[16] R. H. Kraichnan, Helical turbulence and absolute equilibrium, J. Fluid Mech., 59 (1973), 745–752.

[17] R. H. Kraichnan, Statistical dynamics of two-dimensional flows, J. Fluid Mech., 67 (1975), 155–175

[18] R. H. Kraichnan & D. Montgomery, Two-dimensional turbulence, Rep. Prog. Phys., 43 (1980), 547–619.

[19] L. D. Landau & E. M. Lifshitz, Statistical Physics, 3rd Ed., Pergamon, New York (1980), Chap. 1.

[20] L. D. Landau & E. M. Lifshitz, Electrodynamics of Continuous Media, 2nd Ed., Pergamon, New York (1984), Chap. 8.

[21] T. D. Lee, On some statistical properties of hydrodynamical and magneto-hydrodynamical fields, Q. Appl. Math., 10 (1952), 69.

[22] W. H. Matthaeus, W. T. Stribling, D. Martinez, S. Oughton, & D. Montgomery, Decaying, two-dimensional Navier-Stokes turbulence at very long times, Physica D, 51 (1991), 531–538.

[23] H. K. Moffatt, The degree of knottedness of tangled vortex lines, J. Fluid Mech., 35 (1969), 117–129.

[24] A. M. Obukhov, Spectral energy distribution in a turbulent flow, Dokl. Akad. Nauk SSSR, 32 (1941), 22–24.

[25] S. Oughton, E.R. Priest & W.H. Matthaeus, The influence of a mean magnetic field on three-dimensional MHD turbulence, J. Fluid Mech., 280 (1994), 95–117.

[26] R. G. Palmer, Broken ergodicity, Adv. Phys., 31 (1982), 669.

[27] G. S. Patterson & S. A. Orszag, Spectral calculation of isotropic turbulence: Efficient removal of aliasing interaction, Phys. Fluids, 14 (1971), 2538–2541.

[28] R. V. Polovin & V. P. Demutskii, Fundamentals of Magnetohydrodynamics, Consultants Bureau, New York (1990), 237–239.

[29] S. B. Pope, Turbulent flows, Cambridge U. P., Cambridge, UK (2000), Chap. 13.

[30] J. V. Shebalin, Anisotropy in MHD turbulence due to a mean magnetic field, Ph.D. Dissertation, College of William and Mary (1982).

[31] J. V. Shebalin, W. H. Matthaeus, & D. Montgomery, Anisotropy in MHD turbulence due to a mean magnetic field, J. Plasma Phys., 29 (1983), 525–47.

[32] J. V. Shebalin, Broken ergodicity and coherent structure in homogeneous turbulence, Physica D, 37 (1989), 173–191.

[33] J. V. Shebalin, Broken symmetry in ideal magnetohydrodynamic turbulence, Phys. Plasmas, 1 (1994), 541–547.

[34] J. V. Shebalin, Absolute equilibrium entropy, J. Plasma Phys. 56 (1996), 419–427.

[35] J. V. Shebalin, Phase space structure in ideal homogeneous turbulence, Phys. Lett. A, 250 (1998), 319–322.

[36] J. V. Shebalin, The statistical mechanics of ideal homogeneous turbulence, NASA TP-2002-210783, Johnson Space Center, Houston, TX (2002).

[37] T. Stribling & W. H. Matthaeus, Statistical properties of ideal three-dimensional magnetohydrodynamics, Phys. Fluids B, 2 (1990), 1979–1988.

[38] F. F. Verhulst, Nonlinear differential equations and dynamical systems, 2nd Ed, Springer-Verlag, New York (1996), Chap. 2.

[39] L. Woltjer, A theorem on force-free magnetic fields, Proc. Nat. Acad. Sci. USA, 44 (1958), 489–491.

[40] S. J. Zweben and S. S. Medley, Visible imaging of edge fluctuations in the TFTR tokamak, Phys. Fluids B, 1 (1989), 2058–2065.